

DESIGN AND OPTIMIZATION OF A SPIRAL ELECTRODE TRIBOELECTRIC NANOGENERATOR USING RESPONSE SURFACE METHODOLOGY

Mohammadali HEYDARI¹ , Tahereh Fanaei SHEIKHOLESLAMI² ,
Amin BEHZADMEHR² 

¹Department of Electronics Engineering, Faculty of Electrical and Computer Engineering,
University of Sistan and Baluchestan, University Blvd, Zahedan, Iran

²Department of Mechanical Engineering, Faculty of Engineering,
University of Sistan and Baluchestan, University Blvd, Zahedan, Iran

ma.heydari@pgs.usb.ac.ir, tahere.fanaei@ece.usb.ac.ir, amin.behzadmehr@eng.usb.ac.ir

DOI: 10.15598/aece.v20i2.4285

Article history: Received Jul 15, 2021; Revised Mar 16, 2022; Accepted Apr 10, 2022; Published Jun 30, 2022.
This is an open access article under the BY-CC license.

Abstract. *Triboelectric nanogenerator is a promising technology and emerging approach for harvesting environmental mechanical energy. However, because of nature of the environmental mechanical motions, the amplitude and direction of the movements are unpredictable. In this paper, a triboelectric nanogenerator with a zero inductance spiral electrode is proposed to generate electricity from sliding motions, regardless of the motion direction. Various samples with different electrode size and number of spiral electrodes were fabricated and characterized. To obtain the optimum output power density, response surface methodology was employed. The experiments were designed based on the central composite design approach for different combinations of the electrode turn number and the electrode width and pitch. To show the validity and accuracy of the method, the predicted results were compared with additional experimental results which a good concordance between the results. Contours of output power density for different combinations of the design variables were plotted. The latter helps designers to easily find the optimal configuration to obtain the desired power output.*

Keywords

Spiral electrode, TENG, DOE, central composite design, response surface methodology.

1. Introduction

The importance of intelligent wireless systems in modern world has created an increasing need to design and fabricate sustainable power supplies using environmental renewable and clean energies. One of the simplest methods to convert the energy of environmental mechanical motions into the clean electrical energy is based on the intrinsic properties of materials such as piezoelectric and triboelectric.

Triboelectric Nanogenerator (TENG) is one of the important inventions which have been presented in recent years [1] and [2]. Until now, lots of various vertical and sliding types of TENG have been developed, especially, using polymer materials, which made this technology a promising route for producing clean and cheap electrical energy [3], [4], [5] and [6]. Environmental mechanical energies widely exist all around the world. They can be in form of the human and animal body motions or the kinetic energy of wind and ocean waves. To harvest such mechanical energies, proper TENG device for each input energy, depending on its characteristics, should be designed [7].

In a TENG, measurable triboelectric charges are created between the surface of two different materials, when they come in contact and separate [8]. According to the path and direction of the employed mechanical motion, two types of TENG can be used which are worked in sliding or vertical contact-separation modes. In a vertical structure TENG, the transferred triboelec-

tric charges establish an electric potential between the top and bottom electrodes and thus produce an electric current at the external outputs [4]. However, in a sliding TENG, the friction between two triboelectric layers caused by a sliding motion produces the triboelectric charges which are induced in the external electrodes [5].

The two types of TENG device can be fabricated with a single metal electrode to simultaneously play the role of the triboelectric layer and the charge transferring electrode [9] and [10]. However, since the sliding mechanical movements are often variable in amplitude and occur in unpredictable directions [11], designing TENG that can employ such random sliding motions is of great importance. Such a TENG that can produce electrical power independence of the input characteristics is very useful and practical due to its vast applications in harvesting energy from friction-based environmental motions such as all type of body motions or ocean and wind energies. Furthermore, the output of the device should be maximized based on the effective geometrical parameters. The latter is important for successful utilization of the device for the motions with various amplitudes.

A practical and interesting method for optimizing the output power density of a TENG device when optimal design parameters are needed is the Response Surface Methodology (RSM) which is part of the Design of Experiments (DOE). It was originally developed to model experimental responses and to model numerical experiments [12] and [13]. For building an experimental model with RSM, a set of statistical techniques and applied mathematics will be employed. RSM are designed in different ways depending on the experimental design, which one of these methods is a Central Composite Design (CCD) method [14].

The application of RSMs is very wide in industries such as chemical, petrochemical, food, pharmaceutical, microbiology, etc. [13], [14] and [15]. Recently, in a study for tribological performance of sliding polymers, In [16] used RSM method to show the connection between control factors, sliding speeds, the average coefficient of friction, and the wear rate as responses. Also, RSM was also used for optimization and statistical process control of polymer triboelectric charging [17]. However, despite of the powerful methodology of DOE in controlling and optimizing devices and systems, the works that use this approach for optimizing TENG devices are rare.

In this paper, a particular sliding TENG with a single spiral electrode is designed, fabricated, and characterized. The circular form of electrode well respond to harvest the mechanical motions energy irrespective of their direction. RSM was employed to optimize the device performance based on design the experiment

method of CCD. Three geometrical design parameters: the electrode turn number, the electrode width and spiral pitch were considered as design parameters while the power density of TENG was the objective parameter (response).

2. Materials and Methods

As the performance of conventional sliding motion triboelectric nanogenerators is limited by the direction of the sliding layer movement, a circular symmetrical electrode is proposed and designed for TENG device. The structure of the nanogenerator has been schematically shown in Fig. 1(a). In this figure, L and x are the length of the dielectric and the lateral overlapping distance, respectively. Figure 1(b) shows the mechanism of the charge and current generation in the device. The fabricated electrode is shown in Fig. 1(c), where the copper spiral electrode was formed on an epoxy fiberglass (Fr-4) layer using chemical etching. The thickness of the Fr-4 layer and the spiral copper electrode is 1.6 mm and 35 μm , respectively. The triboelectric layers consist of Polyvinylchloride (PVC), with the thickness of 200 μm , and Polyurethane (PU), with the thickness of 2 mm, which produces electric charges when sliding together. Then, the equal charges are inducted on the spiral electrode through PVC layer. It should be indicated that the spiral electrode and the fennel substrate also positively affect the final inducted charge, due to a small vertical movement of the PVC layer over the substrate. The latter is not shown in Fig. 1(b) to avoid complexity of the figure. PVC layer also protects the electrode from abrasion.

The spiral form of the electrode consists of two arms planar Archimedean coil which are connected together so its inductance is negligible. Therefore, the device is not affected by negative effect of the inductance. In the device configuration, PVC layer, spiral electrode and the Fr-4 substrate form the fixed part of the nanogenerator. PU layer as the movable part can slide over the fixed part in all directions. This part is actually connected to moving part of the environmental motion energy source. For example, it can be connected to a sliding mouse on a fixed PVC pad or to the belt of a sports instrument when slides over the body or legs. Moreover, the device can be employed as a self-powered real-time sensor to detect the omnidirectional sliding motions in the mentioned situations.

To apply a similar sliding motion on all the fabricated samples, an environmental motion simulator was fabricated, which is shown in Fig. 1(d). The mechanical motion simulating device includes two parts: fix and moving one. The epoxy fiberglass (Fr-4) layer, spiral electrode and PVC layer were fixed on the fix part while the PU layer was fixed on the moving part

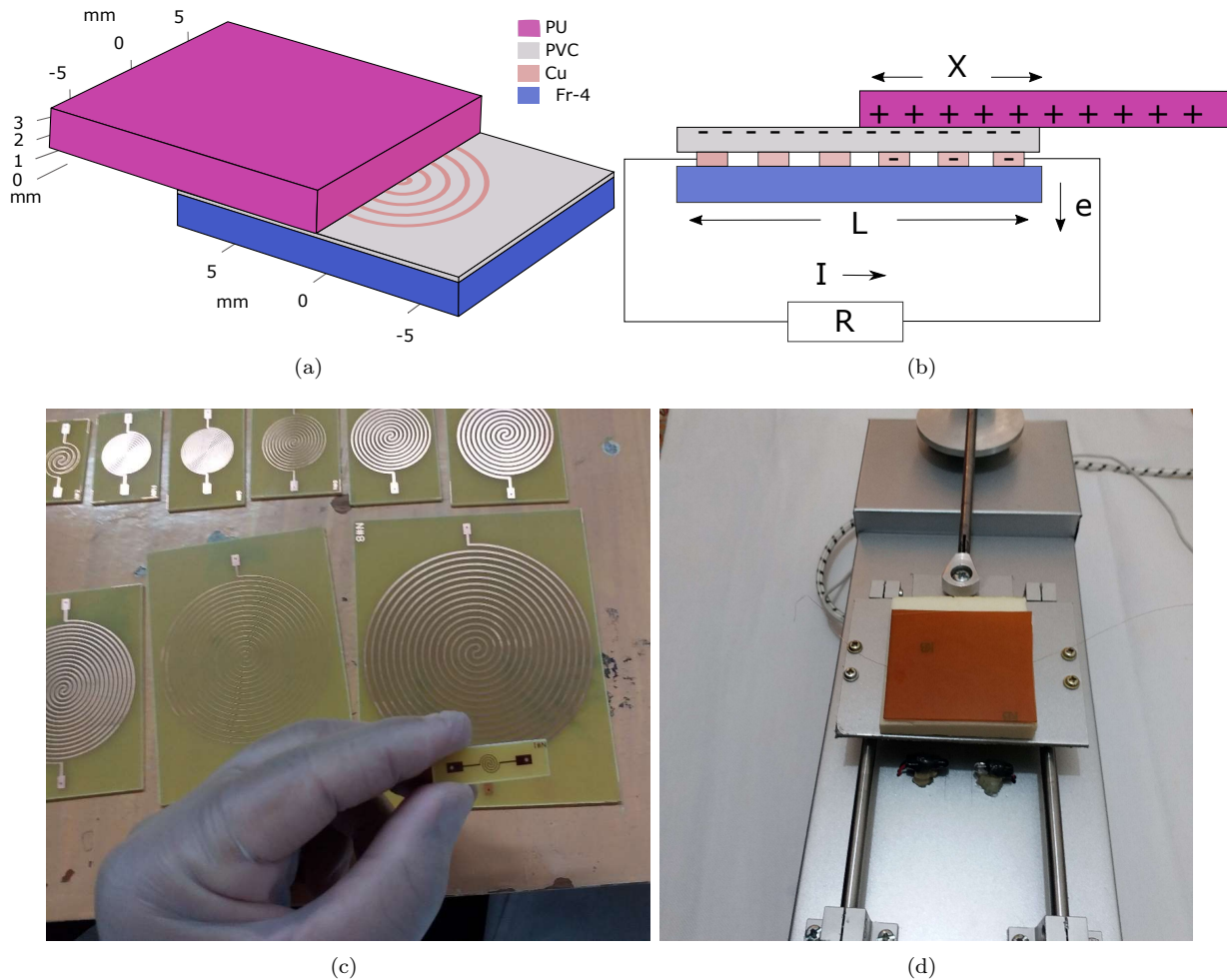


Fig. 1: (a) scheme of the fabricated TENG; (b) spiral electrodes with different turns, (c) the real fabricated device and (d) mechanical motion simulating instrument.

of the device. The moving part controls the moving frequency of motion and also the exerted force on the fix part. In this study, the frequency and exerted forces were adjusted to be 2 Hz and 10 N, respectively.

As the performance of fabricated TENG depends on the number of spiral turns, electrode width, and electrode pitch, different samples are fabricated considering such parameters. To finding suitable configurations of TENG, the DOE approach was adopted for the investigations. Therefore, the experimental tests were designed and carried out based on the approach to find the direct effect of triboelectric main parameters as well as their interactions on the nanogenerator performance.

DOE is an effective and flexible statistical approach for optimizing the performance of the device at various conditions. For this purpose, among different methods, the RSM is adopted. The RSM uses a set of statistical techniques to design the experimental models.

The RSM can be designed considering different approaches, for example, central composite design and

Box-Behnken Design (BBD) are the two popular factorial designs. These design approaches make it possible to achieve second-order polynomial models in RSM. Differences in levels between CCD and BBD methods result from differences in the number of experiments. In the case of experiments with up to five levels, the CCD is more efficient.

Thus to investigate the effects of turn number, electrode width, and electrode pitch on the nanogenerator performance the CCD method is adopted to construct the test conditions. These parameters and their lower and upper levels are shown in Tab. 1.

Tab. 1: Independent variables and their levels.

Variable	Symbol	Units	Low	High
Electrode Width	X_1	mm	0.25	1
Electrode Pitch	X_2	mm	0.5	2
Turn number	X_3	-	4	16

The response (power density of nanogenerator) was measured and analyzed using response surface methodology. The response can be modelled considering

a second-order polynomial equation as follows:

$$Y = b_0 + \sum_{i=1}^k b_i x_i + \sum_{i=1}^{k-1} \sum_{j=2}^k b_{ij} x_i x_j + \sum_{i=1}^k b_{ii} x_i^2, \quad (1)$$

where Y is the predicted response (power density of nanogenerator), x_i , x_j are independent factors (electrode width, and the electrode pitch, and the turn number), b_0 is the intercept coefficient, b_i is the linear effect, b_{ij} is the interaction effect, b_{ii} is the quadratic effect, and k is the number of variables. Analysis of Variance (ANOVA) was also conducted to determine the significance of the main parameters and their interaction.

3. Results

3.1. Basic Mechanism

The basic mechanism of the power generation by the spiral TENG is believed to be due to the presented triboelectric couple surfaces of, PU/PVC, PVC/Fr-4 (Epoxy), and PVC/CU. Referring to the triboelectric series table [9], the order of electronegativity increasing is as PVC > Cu > Epoxy > PU. The majority of triboelectric charges are produced between PU and PVC. Then they are induced as the negative charges on the copper spiral electrode when positively charged sliding PU is overlapped with spiral electrode (see Fig. 2(a)).

As it is shown in Fig. 2, when there is No Overlap (NO) between PU and the fixed substrate and also, when there is Fully Overlapped (FO) situation, no current flows. In other situations, negative charges are induced only in a part of the coil that is under the positively charged PU layer. As a result, the remained parts of the coil will lose some negative charges to resume the equilibrium condition which results the charges flowing in the external circuit (Fig. 2(a)).

In Half overlapping (HF), the current has a maximum value. Due to the small gap between PVC and substrate, the triboelectric charges can also be produced between PVC/Fr-4 and between PVC/Cu, when they are in contact (as result of exerted forces). The latter induced positive charges on copper electrode when they are separated. These charges are added to the induced charges from the first mechanism and produce the output current in a same direction.

3.2. Current and Voltage Responsesm

Figure 3 and Fig. 4 present the effect of spiral turn number on the nanogenerator performance. The output current and voltage of the device were measured

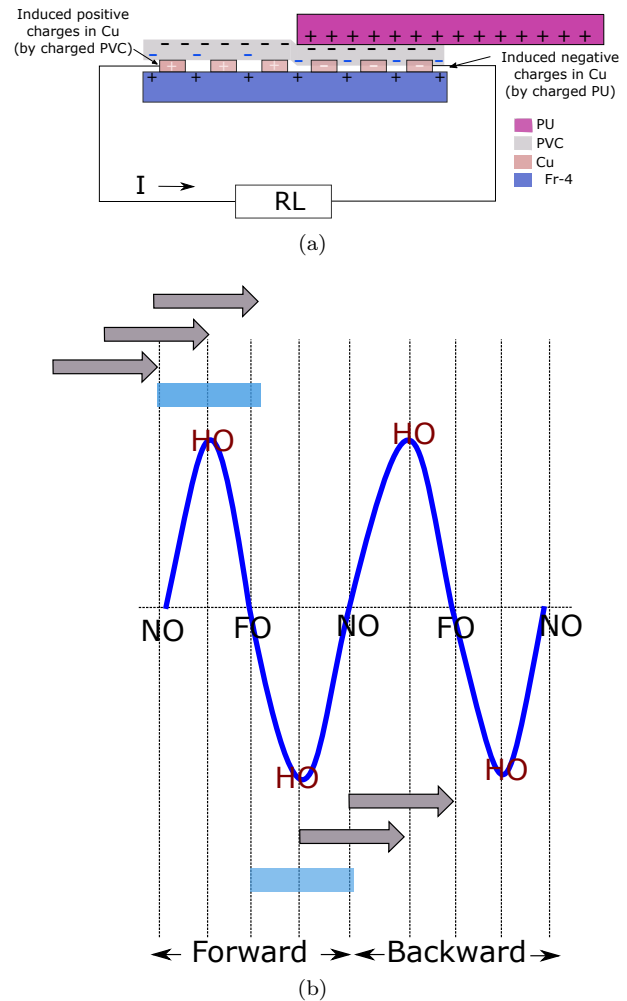


Fig. 2: Power generation mechanism of TENG; a) Charges production mechanism (dimensions are not at scale) and b) Output signal in forward and backward movements.

over a 0.1 MΩ load. Figure 3 shows the effect of spiral turn number of 4, 8, 16 and 20 on the output current of the nanogenerator. In all the presented measurements, the electrode width and electrode pitch were 0.25 mm and 1.5 mm, respectively. As can be seen, the current density augments with increasing the spiral turn number. The same behaviour is observed for the output voltage which is shown in Fig. 4. The average peak to peak values of the given outputs are given in Tab. 2.

Tab. 2: The average peak to peak values for the measured currents and voltages shown in Fig. 3.

Variable	4-Turns	8-Turns	16-Turns	20-Turns
V_{P-P} (mV)	60	85	120	200
I_{P-P} (μA)	0.3	0.6	0.9	1.6

As the outputs are AC signals, the electrical power density that is produced by the device is calculated by multiplying the root mean square of the measured current and voltage and dividing by the effective area

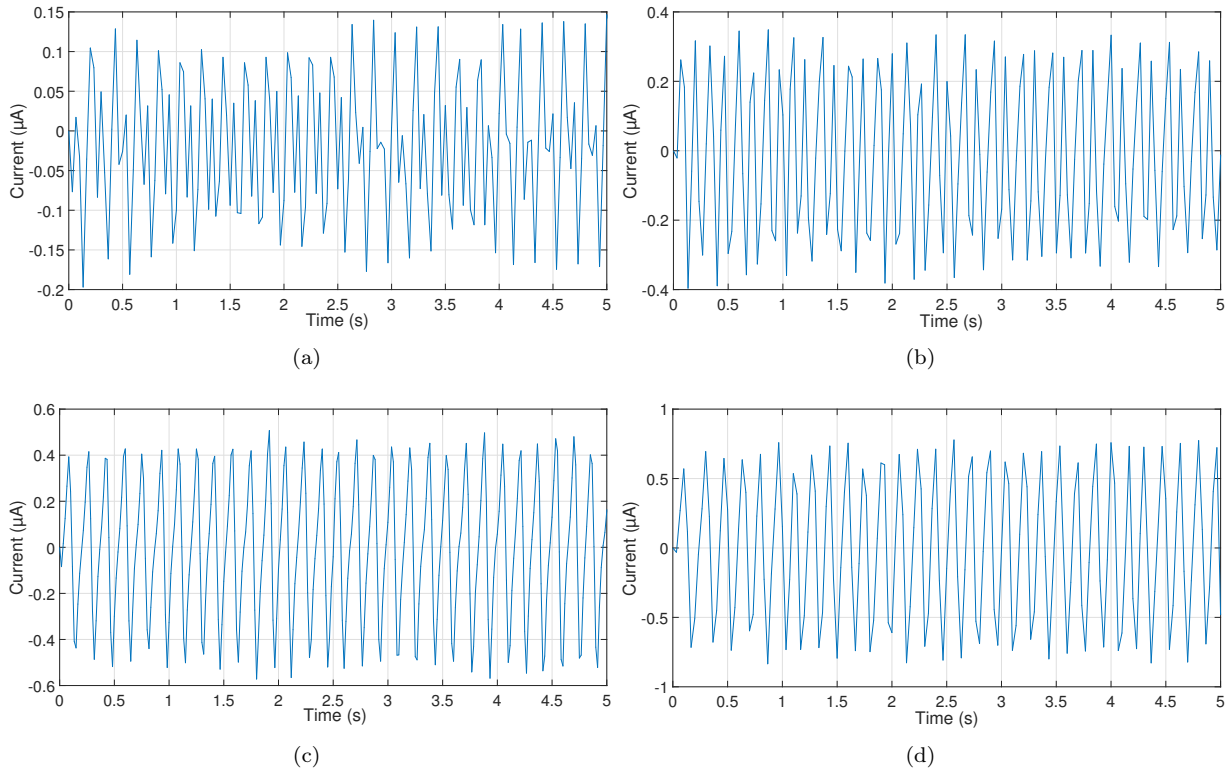


Fig. 3: The instantaneous current measured in the proposed TENG; a) 4, b) 8, c) 16 and d) 20, turns of the electrode.

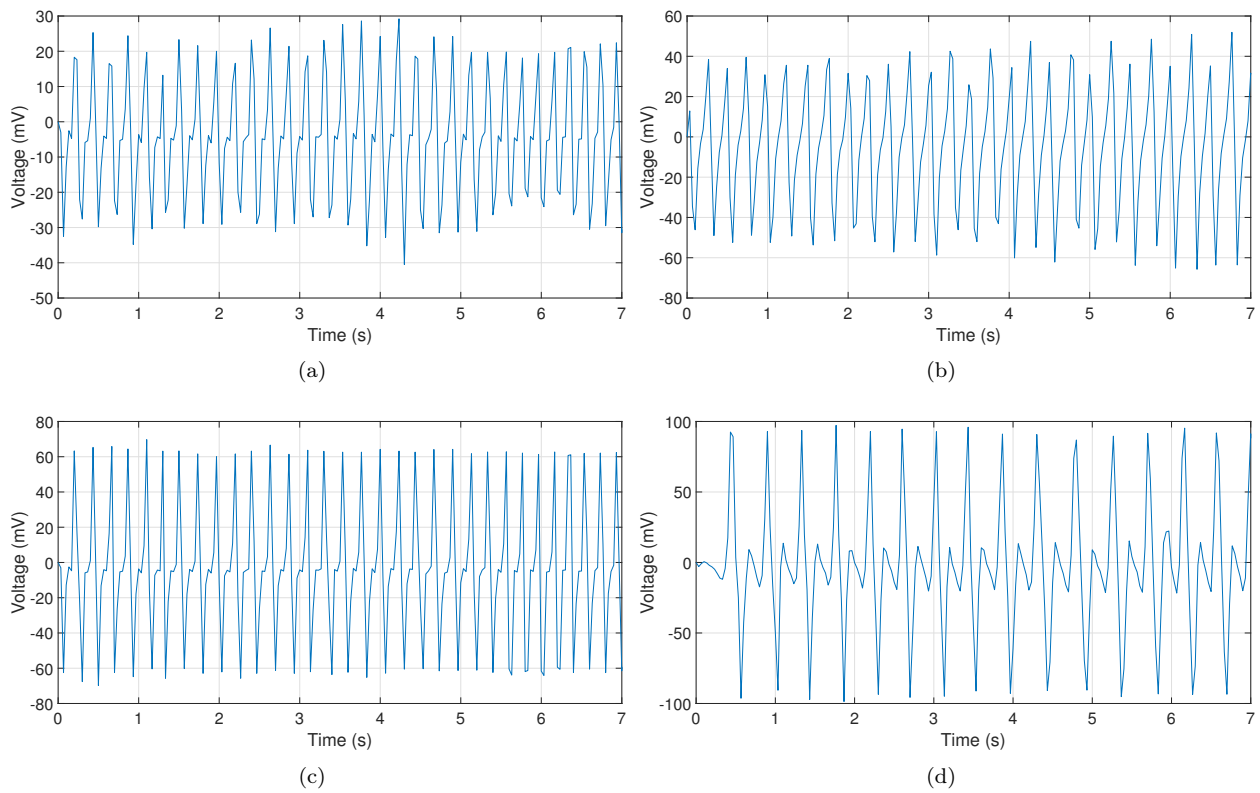


Fig. 4: The instantaneous voltage measured in the proposed TENG; a) 4, b) 8, c) 16 and d) 20, turns of the electrode.

of each device. The results are reported as the output power density in the following sections.

To explore and understand the performance of nanogenerator with all the combinations of spiral turn number, electrode width and electrode pitch response surface methodology is used for further experiments.

3.3. Response Surface Analysis and Interpretation

CCD approach is adopted to construct a table of the experimental runs. It was performed based on the eight factorial points, six axial points, and three center points that resulted in a total of 17 experimental runs. These experimental runs and their responses (power density) are presented in Tab. 3.

Multiple regression was used to obtain the second-order polynomial equation in terms of significant independent factors and their interaction. It is defined by Eq. (2). As can be noticed, the power density of the nanogenerator is predicted for different combinations of electrode width, the electrode pitch, and the spiral turn number by using Eq. (2).

$$(Y)^{0.44} = 13.6417 + 23.3234X_1 - 18.4853X_2 + 0.0458883X_3 + 18.3014X_1X_2 - 1.88904X_1X_3 + 0.171245X_2X_3 - 36.1282X_1^2 + 6.75349X_2^2 - 0.31483X_1X_2X_3 + 9.5334X_1^2X_2 + 2.02536X_1^2X_3 - 10.4299X_1X_2^2. \quad (2)$$

Tab. 3: CCD experimental design matrix and experimental responses.

Run	X_1 (mm) electrode width	X_2 (mm) electrode pitch	X_3 turn number	Power Density, ($\mu\text{W}\cdot\text{m}^{-2}$)
1	0.25	0.5	4	212.769
2	1	0.5	4	39.2956
3	0.25	2	4	75.583
4	1	2	4	29.0848
5	0.25	0.5	16	98.4187
6	1	0.5	16	66.8582
7	0.25	2	16	44.841
8	1	2	16	13.5301
9	0.25	1.25	10	42.9295
10	1	1.25	10	78.6943
11	0.625	0.5	10	145.988
12	0.625	2	10	30.1073
13	0.625	1.25	4	140.03
14	0.625	1.25	16	27.3913
15	0.625	1.25	10	71.235
16	0.625	1.25	10	74.2185
17	0.625	1.25	10	70.5735

ANOVA was performed to show the model suitability and also to present the significance of each parameter and their interaction. Its results are presented in Tab. 4. The p-value less than 0.05 indicates model terms are significant. The coefficient of regression (R-squared) is 0.9997 which is close to 1. It indicates that the experimental and predicted responses are well correlated.

Tab. 4: ANOVA for response surface quadratic model.

Source	Sum of Squares	df	Mean Square	F-value	p-value
Model	58.37	12	4.86	1325.47	< 0.0001
X_1	1.28	1	1.28	347.88	< 0.0001
X_2	10.07	1	10.07	2742.86	< 0.0001
X_3	10.15	1	10.15	2766.72	< 0.0001
$X_1 X_2$	0.6267	1	0.6267	170.78	0.0002
$X_1 X_3$	2.51	1	2.51	684.94	< 0.0001
$X_2 X_3$	0.1055	1	0.1055	28.76	0.0058
X_1^2	0.9382	1	0.9382	255.66	< 0.0001
X_2^2	0.0528	1	0.0528	14.40	0.0192
$X_1 X_2 X_3$	2.26	1	2.26	615.35	< 0.0001
$X_1^2 X_2$	1.62	1	1.62	440.81	< 0.0001
$X_1^2 X_3$	4.67	1	4.67	1273.32	< 0.0001
$X_1 X_2^2$	7.74	1	7.74	2110.45	< 0.0001
Residual	0.0147	4	0.0037		
Lack of Fit	0.0026	2	0.0013	0.2184	0.8208
Pure Error	0.0120	2	0.0060		
$R^2 = 0.9997$, $R_{adj}^2 = 0.9990$, adequate precision = 140.24 (> 4)					

1) Model Reliability

Predicted vs. Actual graph in Fig. 5 shows whether the generated equation of the response surface accurately predicts the actual experimental values. As can be observed, all the measured values (that are used for modelling) are well correlated with the predicted model. Therefore, the generated response surface model can be considered as reliable.

2) DOE Results

Figures 6, Fig. 7 and Fig. 8 are plotted based on the response surface modelling that is related to the DoE concept. These contours are used to observe the relationship between the power density (as a response variable) and the design parameters such as electrode turn number, electrode pitch and electrode width (as experimental factors). Such an approach helps to find the optimized geometrical parameters that can result the highest output power density through the use of the different spiral electrode configurations.

The power density contours in terms of variations in the electrode width and pitch are plotted in Fig. 6. Figure 6(a) and Fig. 6(b) show the power density variations for the device with 4 and 16-turns spiral electrodes, respectively.

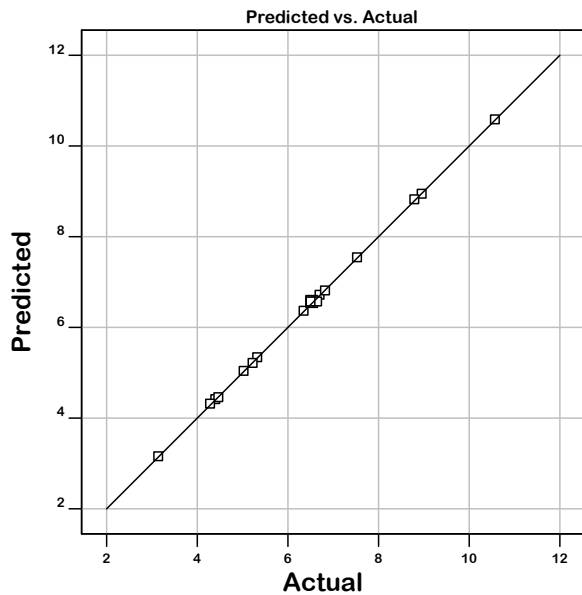


Fig. 5: Comparison between the predicted results and actual results.

Furthermore, the device power density contours for two different pitches of the spiral electrode, equal to 0.5 and 2.0 mm, are plotted in Fig. 7(a) and Fig. 7(b), in terms of the variations in the electrode width and the spiral turns number.

Finally, to find the effect of changing in the turn's number and the electrode pitch together, while a constant electrode width is used, the power density contours are plotted in Fig. 8 for different electrode pitches and various turn number of the spiral electrodes. The results are obtained for two different widths of the spiral electrode, equal to 0.25 and 1.0 mm, which are plotted in Fig. 8(a) and Fig. 8(b), respectively.

4. Discussion

To assess the precision of the model on the prediction of power density, comparisons with the new experimental results within and outside of the lower level and upper level were performed. As shown in Tab. 6, within the range where the experimental results are carried out, is 4.89 % is the maximum difference between the predicted results and new measured results. However, the difference between the results outside of the considered range is about 9.16 %. Thus, the model accuracy for predicting within the range is very high while for the outside of the considered range is acceptable.

Considering Fig. 5, the horizontal axis corresponds to the actual values measured in the experimental work and the vertical axis shows the predicted values by the software based on statistical data. The measured values according to Tab. 3 are applied to the software and

the predicted values are obtained using Eq. (2), which is the output of statistical calculations of the software. Figure 5 shows a comparison between these values.

It can be observed that there is a good agreement between the results. It confirms that the model accuracy for predicting within the range is very good while for the outside of the considered range it is acceptable.

Based on the performed analysis, it can be concluded that the electrode geometrical parameters have significant effects on the produced output power by the spiral electrode TENG.

The extracted contours in Fig. 6 indicate that the power density of the device is decreased for higher spiral turns. It can be attributed to a higher variation in source sliding velocity when a larger area is scanned. However, the secondary effects such as low-pressure contacts between the surfaces will also decrease the output power density. However, by adjusting the electrode width and pitch, as it is proposed by DOE results, the power density decreasing can be partially compensated.

The maximum power density is obtained for a 2-turns device, when the electrode width varies between 0.18 to 0.58 mm while the electrode pitch is in the range of 0.2 to 0.35 mm. Increasing the electrode pitch higher than 0.35 mm decreases the power density of the device. In a 16-turns device, the highest power density is obtained when the electrode width is in the range of 0.1 to 0.25 mm while the electrode pitch varies in the range of 0.2 to 0.27 mm. Fig. 7(a) shows the effects of different combinations of spiral electrode turn number and electrode width for the electrode pitch of 0.5 mm while Fig. 7(b) shows this combination for the electrode pitch of is 2.0 mm. As can be noticed, it is possible to obtain a higher power density when the lower electrode width is selected. Fig. 8 indicated that for a device with smaller electrode width, a higher power density is obtained at low electrode pitch, while in the case of higher electrode width, the higher-power densities are shifted around the electrode with the pitch of 1 mm.

The results show that there are different combinations that lead to the desired power density. Based on the above-mentioned mechanism, if the electrode pitch is increased, a higher power density is expected, however, in very high pitches, the collecting of charges by electrode reduces which leads to decrease in the output power density again.

4.1. Performance Comparison

In order to compare the performance of different triboelectric nanogenerators that have been recently developed with the presented model, Tab. 5 is presented.

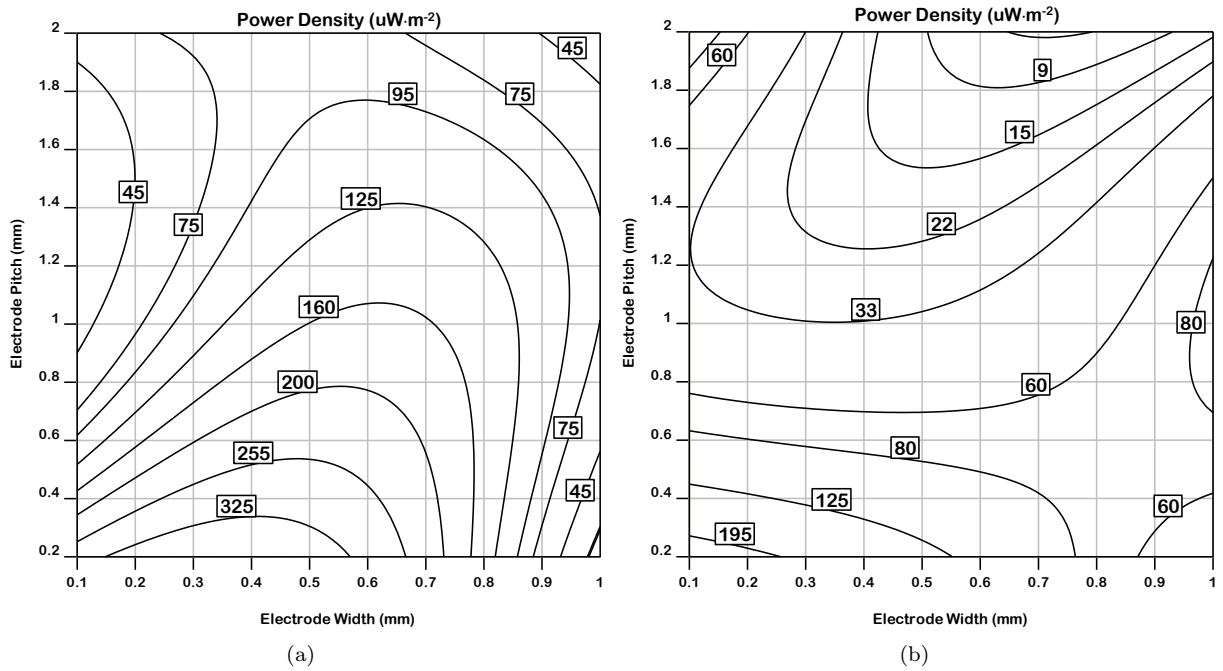


Fig. 6: 2D Contour plots of power density based on various combinations of electrode pitch and electrode width a) 4-turns spiral electrode and b) 16-turns spiral electrode.

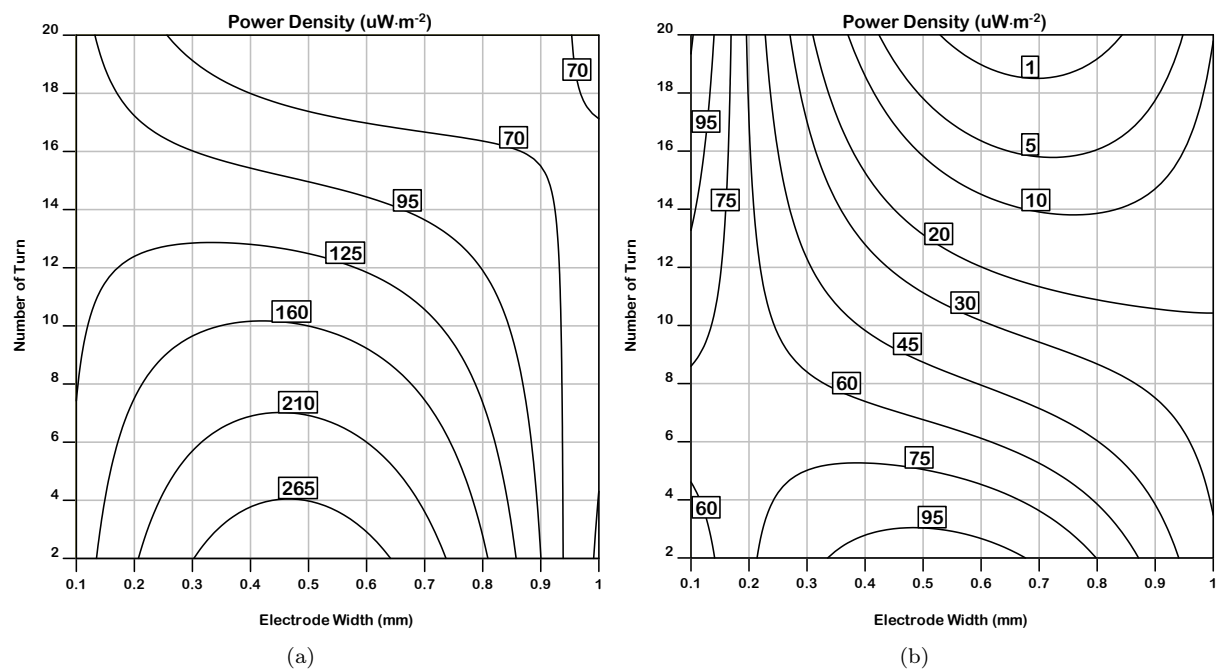


Fig. 7: 2D Contour plots of power density based on various combinations of spiral electrode turn number and electrode width a) 0.5 mm electrode pitch and b) 2.0 mm electrode pitch.

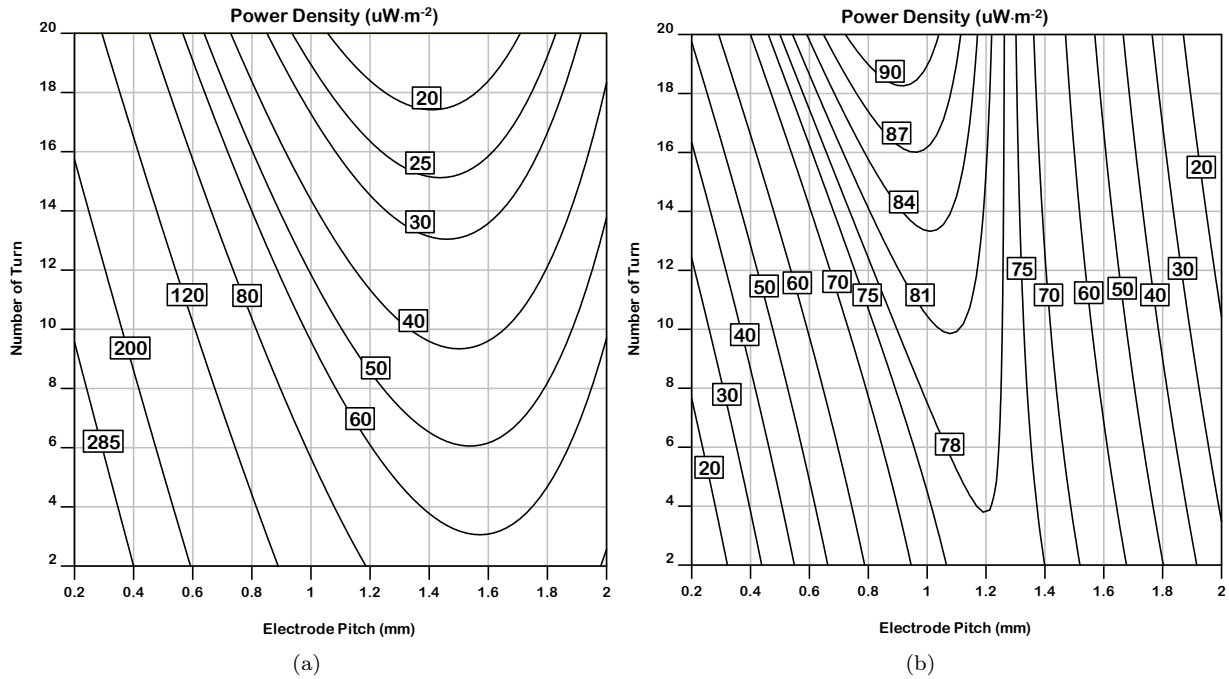


Fig. 8: 2D Contour plots of power density based on various combinations of spiral electrode turn number and electrode pitch a) 0.25 mm electrode width and b) 1.0 mm electrode width.

Tab. 5: Comparison between the present work and some recent developed TENGs.

Type of Device	Best Outputs	Considered Parameters	Moving Direction	Year
Sliding Spiral Steel Wire	$P = 2.13 \mu\text{W}$, $L = 6 \text{ cm}$ and $d = 3 \text{ mm}$	Frequency, External loads, Strain	Along the cylinder	2019 [18]
Sliding Grating Electrode	$P = 3.6 \text{ mW}$, Size: $3.5 \times 3.5 \text{ cm}$, line density = $600 \cdot \text{mm}^{-1}$	Surface Plasmon excitation, Line numbers, Light	Vertical	2019 [19]
Sliding Archimedes Spiral Electrodes	$V_{oc} = 10 V_{p-p}$	Rotation angle, Number of electrodes	2D Multi-direction	2021 [20]
Single Electrode Vertical TENG	$V_{oc} = 21.63 \text{ V}$,	Surface microstructure	Vertical	2022 [21]
Two Electrode Sliding Droplet Based	$Q_{sc} = 197 \text{ pC}$, $d = 1.2 \text{ cm}$, Simulated result	Frequency, Height of droplet release	Surface slope	2022 [22]
Two Electrode Vertical TENG	$I_{sc} = 0.48 \mu\text{A}$ for one droplet	Surface structure, Humidity and impurity resistance	Vertical	2022 [23]
Sliding Archimedean Single Spiral	$V_{oc} = 60 \text{ V}$	Spiral turns, Width and Pitch of the electrode	2D Multi-direction	Proposed study

Tab. 6: ANOVA for response surface quadratic model.

Electrode width (mm)	Electrode pitch (mm)	Turn number	Measured ($\mu\text{W} \cdot \text{m}^{-2}$)	Predicted ($\mu\text{W} \cdot \text{m}^{-2}$)	Deviation (%)
0.25	0.5	8	9.740	9.566	1.79
0.25	1.5	8	9.566	9.256	3.24
0.5	1.75	10	5.459	5.138	4.89
0.25	1.5	20	3.556	3.352	5.73
0.25	0.5	20	7.120	6.524	8.38
2	1.5	10	5.757	5.230	9.16

As mentioned before, one of the advantages of the presented TENG is its functional ability regardless the direction of the motion which is not reported by other TENGs. There is a work introduced in [20] that also used multiple Archimedes spiral electrodes for motion detection, where its multidirectional performance makes it possible to be used for motion detection. In spite of such an advantage of the proposed study, the output power of the presented work is similar or lower than of some given works in the Tab. 5. However, the comparison of the output power cannot be made with the ones who have reported the open circuit voltage or short circuit current.

5. Conclusion

In this paper, a TENG with spiral electrodes was designed and fabricated to harvest energy from random and unpredictable movements in the environment. The designed nanogenerator has a symmetrical structure so its performance is not affected by the direction of the sliding environmental motions. However, the environmental sliding motion, inherently, has various amplitudes that affect the geometrical parameter of a designed TENG. To optimize the nanogenerator performance for different combinations of geometrical parameters, a response surface methodology was adopted. The latter include the turn number of spiral electrodes, electrode width and electrode pitch. The experiments were designed based on the central composite design approach and the output power density is considered as a response parameter. For different combinations of the turn number of spiral electrodes, electrode width and electrode pitch, contours of power density were plotted. These contours help the designer to easily find the optimal situation for different applications. Multiple regression was used to fit a second-order polynomial equation for prediction the power density in terms of design variables. When comparing the predicted values with the experimental results (that are not used for developing the RSM), good concordance was observed. Desirability analysis shows that it is possible to obtain power density equal to $212.997 \mu\text{W} \cdot \text{m}^{-2}$ when the electrode width of 0.25 mm, electrode pitch of 0.5 mm and 4-turns spiral electrode are considered.

Author Contributions

M.H. carried out the experimental work and performed the DoE analysis. T.F. verified the experimental work and A.B. verified the DoE analysis. Both T.F. and A.B. supervised the project and revised the first draft of manuscript that was written by M.H.

References

- [1] SLABOV, V., S. KOPYL, M. P. SOARES DOS SANTOS and A. L. KHOLKIN. Natural and Eco-Friendly Materials for Triboelectric Energy Harvesting. *Nano-Micro Letters*. 2020, vol. 12, iss. 42, pp. 1–18. ISSN 2150-5551. DOI: 10.1007/s40820-020-0373-y.
- [2] TIAN, J, X. CHEN and Z. L. WANG. Environmental energy harvesting based on triboelectric nanogenerators. *Nanotechnology*. 2020, vol. 31, iss. 24, pp. 1–66. ISSN 0957-4484. DOI: 10.1088/1361-6528/ab793e.
- [3] BEKKARA, M. F., L. DASCALESCU, Y. BENMIMOUN, T. ZEGHLOUL, A. TILMATINE and N. ZOUZOU. Modification of surface characteristic and tribo-electric properties of polymers by DBD plasma in atmospheric air. *The European Physical Journal Applied Physics*. 2018, vol. 81, iss. 1, pp. 1–9. ISSN 1286-0050. DOI: 10.1051/ep-jap/2017170149.
- [4] YANG, B., W. ZENG, Z. PENG, S. LIU, K. CHEN and X. TAO. Polymer chemistry underpinning materials for triboelectric nanogenerators (TENGs): Recent trends. *European Polymer Journal*. 2021, vol. 142, iss. 1, pp. 1–8. ISSN 1614-6840. DOI: 10.1002/aenm.201600505.
- [5] DZHARDIMALIEVA, G. I., B. C. YADAV, T. V. LIFINTSEVA and I. E. UFLYAND. Polymer chemistry underpinning materials for triboelectric nanogenerators (TENGs): Recent trends. *European Polymer Journal*. 2021, vol. 142, iss. 1, pp. 1–42. ISSN 0014-3057. DOI: 10.1016/j.eurpolymj.2020.110163.

- [6] LENG, Q., H. GUO, X. HE, G. LIU, Y. KANG, C. HU and Y. XI. Flexible interdigital-electrodes-based triboelectric generators for harvesting sliding and rotating mechanical energy. *Journal of Materials Chemistry A*. 2014, vol. 2, iss. 45, pp. 19427–19434. ISSN 2050-7496. DOI: 10.1039/C4TA04137B.
- [7] HUANG, P., D. WEN, Y. QIU, M. YANG, C. TU, H. ZHONG and X. ZHANG. Textile-Based Triboelectric Nanogenerators for Wearable Self-Powered Microsystems. *Micromachines*. 2021, vol. 12, iss. 2, pp. 1–21. ISSN 2072-666X. DOI: 10.3390/mi12020158.
- [8] BORJESSON, A. A method for measurement of triboelectric charging. In: *Electrical Overstress/Electrostatic Discharge Symposium Proceedings*. Phoenix: IEEE, 1995, pp. 253–261. ISBN 1-878303-59-7. DOI: 10.1109/EOESD.1995.478293.
- [9] ZOU, H., L. GUO, H. XUE, Y. ZHANG, X. SHEN, X. LIU, P. WANG, X. HE, G. DAI, P. JIANG, H. ZHENG, B. ZHANG, C. XU and Z. L. WANG. Quantifying and understanding the triboelectric series of inorganic non-metallic materials. *Nature Communications*. 2020, vol. 11, iss. 1, pp. 1–7. ISSN 2041-1723. DOI: 10.1038/s41467-020-15926-1.
- [10] KAUR, N., J. BAHADUR, V. PANWAR, P. SINGH, K. RATHI and K. PAL. Effective energy harvesting from a single electrode based triboelectric nanogenerator. *Scientific Reports*. 2016, vol. 6, iss. 1, pp. 1–9. ISSN 2045-2322. DOI: 10.1038/srep38835.
- [11] SOUZA, C. R. DE., M. T. BETELLI, P. S. TAKAZONO, J. A. DE OLIVEIRA, D. B. COELHO, J. DUYSSENS and L. A. TEIXEIRA. Evaluation of balance recovery stability from unpredictable perturbations through the compensatory arm and leg movements (CALM) scale. *PLOS ONE*. 2019, vol. 14, iss. 8, pp. 1–17. ISSN 1932-6203. DOI: 10.1371/journal.pone.0221398.
- [12] MONTGOMERY, D. C. *Design and Analysis of Experiments*. 10th ed. New York: Wiley, 2019. ISBN 978-1-119-49244-3.
- [13] BOWDEN, G. D., B. J. PICHLER and A. MAURER. A Design of Experiments (DoE) Approach Accelerates the Optimization of Copper-Mediated 18F-Fluorination Reactions of Arylstannanes. *Scientific Reports*. 2019, vol. 9, iss. 1, pp. 1–9. ISSN 2045-2322. DOI: 10.1038/s41598-019-47846-6.
- [14] BAYUO, J., M. A. ABUKARI and K. B. PELIGBA. Optimization using central composite design (CCD) of response surface methodology (RSM) for biosorption of hexavalent chromium from aqueous media. *Applied Water Science*. 2020, vol. 10, iss. 1, pp. 1–12. ISSN 2190-5495. DOI: 10.1007/s13201-020-01213-3.
- [15] ALMEIDA, D. G., R. DE C. F. S. DA SILVA, J. M. LUNA, R. D. RUFINO, V. A. SANTOS and L. A. SARUBBO. Response Surface Methodology for Optimizing the Production of Biosurfactant by *Candida tropicalis* on Industrial Waste Substrates. *Frontiers in Microbiology*. 2017, vol. 8, iss. 1, pp. 1–13. ISSN 1664-302X. DOI: 10.3389/fmicb.2017.00157.
- [16] CHANG, B. P., H. M. AKIL, R. B. NASIR and A. KHAN. Optimization on wear performance of UHMWPE composites using response surface methodology. *Tribology International*. 2015, vol. 88, iss. 1, pp. 252–262. ISSN 0301-679X. DOI: 10.1016/j.triboint.2015.03.028.
- [17] DASCALESCU, L., K. MEDLES, S. DAS, M. YOUNES, L. CALIAP and A. MIHALCIOIU. Using Design of Experiments and Virtual Instrumentation to Evaluate the Tribocharging of Pulverulent Materials in Compressed-Air Devices. *IEEE Transactions on Industry Applications*. 2008, vol. 44, iss. 1, pp. 3–8. ISSN 1939-9367. DOI: 10.1109/TIA.2007.912801.
- [18] XIE, L., X. CHEN, Z. WEN, Y. YANG, J. SHI, C. CHEN, M. PENG, Y. LIU and X. SUN. Spiral Steel Wire Based Fiber-Shaped Stretchable and Tailorable Triboelectric Nanogenerator for Wearable Power Source and Active Gesture Sensor. *Nano-Micro Letter*. 2019, vol. 11, iss. 1, pp. 1–10. ISSN 2150-5551. DOI: 10.1007/s40820-019-0271-3.
- [19] GAO, L., X. CHEN, S. LU, H. ZHOU, W. XIE, J. CHEN, M. QI, H. YU, X. MU, Z. L. WANG and Y. YANG. Enhancing the Output Performance of Triboelectric Nanogenerator via Grating-Electrode-Enabled Surface Plasmon Excitation. *Advanced Energy Materials*. 2019, vol. 9, iss. 44, pp. 1–11. ISSN 1614-6832. DOI: 10.1002/aenm.201902725.
- [20] GUO, H., H. WANG, Z. XIANG, H. WU, J. WAN, C. XU, H. CHEN, M. HAN and H. ZHANG. Soft Human–Machine Interface with Triboelectric Patterns and Archimedes Spiral Electrodes for Enhanced Motion Detection. *Advanced Energy Materials*. 2021, vol. 31, iss. 34, pp. 1–10. ISSN 1616-3028. DOI: 10.1002/adfm.202103075.

- [21] MATHEW, A. A. and S. VIVEKANANDAN. Design and Simulation of Single-Electrode Mode Triboelectric Nanogenerator-Based Pulse Sensor for Healthcare Applications Using COMSOL Multiphysics. *Energy Technology*. 2022, vol. 10, iss. 5, pp. 1–12. ISSN 2194-4296. DOI: 10.1002/ente.202101130.
- [22] XU, W., X. LI, J. BRUGGER and X. LIU. Study of the enhanced electricity output of a sliding droplet-based triboelectric nanogenerator for droplet sensor design. *Nano Energy*. 2022, vol. 98, iss. 1, pp. 1–7. ISSN 2211-2855. DOI: 10.1016/j.nanoen.2022.107166.
- [23] LI, W., E. LU, A. G. P. KOTTAPALLI and Y. T. PEI. Bioinspired sweat-resistant wearable triboelectric nanogenerator for movement monitoring during exercise. *Nano Energy*. 2022, vol. 95, iss. 1, pp. 1–11. ISSN 2211-2855. DOI: 10.1016/j.nanoen.2022.107018.

About Authors

Mohammadali HEYDARI (corresponding author) received his M.Sc. in Electrical Engineering from Gilan University, Iran in 2015. Now he is pursuing his Ph.D. degree in Electrical Engineering at the University of Sistan and Baluchestan.

Tahereh FANAEI SHEIKHOESLAMI received M.Sc. and Ph.D degree in Electrical Engineering, Microelectronic from University of Sherbrooke, Canada in 2003 and 2008, respectively. Now she is an associate professor at University of Sistan and Baluchestan, Iran. Her research is focused on the MEMS and NEMS design and fabrication.

Amin BEHZADMEHR received M.Sc., degree from Tabriz University, Iran in 1995, and Ph.D. from University of Sherbrooke, Canada in 2003 in Mechanical Engineering. Now he is a full professor at University of Sistan and Baluchestan, Iran. His research focus is on energy and nanotechnology.